




## RESEARCH ARTICLE

## Reaction Engineering, Kinetics and Catalysis

## Modeling enzymatic and electrochemical cascade reactions at the three-phase interface enzyme electrode

Siyu Zou<sup>1</sup>  | Jie Xiao<sup>1,2</sup>  | Xinjian Feng<sup>1</sup> <sup>1</sup>College of Chemistry, Chemical Engineering and Materials Science, Soochow University, Suzhou, Jiangsu Province, China<sup>2</sup>School of Chemical and Environmental Engineering, Soochow University, Suzhou, Jiangsu Province, China

## Correspondence

Xinjian Feng and Jie Xiao, College of Chemistry, Chemical Engineering and Materials Science, Soochow University, Suzhou, Jiangsu Province 215123, China.  
Email: [xjfeng@suda.edu.cn](mailto:xjfeng@suda.edu.cn) and [jie.xiao@suda.edu.cn](mailto:jie.xiao@suda.edu.cn)

## Funding information

National Key Research and Development Program of China, Grant/Award Number: 2019YFA0709200; National Natural Science Foundation of China, Grant/Award Numbers: 21988102, 21978184; Jiangsu Funding Program for Excellent Postdoctoral Talent, the Priority Academic Program Development of Jiangsu Higher Education Institutions (PAPD); Project of Scientific and Technologic Infrastructure of Suzhou, Grant/Award Number: SZS201905

## Abstract

The enzyme electrode based on enzymatic and electrochemical cascade reactions is a golden approach for detecting various biomarkers. How the interfacial architectures of a promising three-phase interface enzyme electrode can influence the cascade reactions and electrode performance, however, remains unclear. In this study, a mathematical model has been developed to describe intraphase and interphase mass transfer, coupled with cascade reactions. The results reveal that the interfacial architectures determine the mass transfer of oxygen (substrate of oxidase) and H<sub>2</sub>O<sub>2</sub> (enzymatic product) in the cascade reactions, hence affecting the electrode current. Generally, thinner pore walls facilitate the mass transfer of oxygen, thereby enhancing the enzymatic kinetics and H<sub>2</sub>O<sub>2</sub> production. Meanwhile, smaller pore sizes shorten the diffusion pathway of H<sub>2</sub>O<sub>2</sub> to the electrode surface, thereby increasing the electrocatalytic reaction rate. This work provides an efficient *in silico* tool for the design of high-performance three-phase enzyme electrodes.

## KEYWORDS

cascade reaction, enzymatic and electrochemical reactions, enzyme electrode, mathematical modeling, three-phase interface

## 1 | INTRODUCTION

The accurate detection of biomarkers (e.g., glucose, lactate, uric acid, protein, etc.) is essential for the diagnosis and treatment of many diseases.<sup>1–7</sup> The development of fast and accurate biomarker detection techniques has long been a focus of research in areas such as biomedicine. Electrochemical enzyme electrodes<sup>8</sup> have the advantages of mild reaction conditions, high selectivity, and high reaction efficiency, and they are widely used in biomarker detection applications.

In oxidase-based enzyme electrodes, oxidases consume oxygen and substrate (analyte) to produce H<sub>2</sub>O<sub>2</sub>. Subsequently, the H<sub>2</sub>O<sub>2</sub> undergoes electrocatalysis on the electrode surface to generate a response current. The enzymatic and succeeding electrochemical reactions form a cascade reaction. Sufficient oxygen supply is a crucial prerequisite for enhancing the enzymatic kinetics. Conventionally, the enzymatic reaction occurs in the solid-liquid two-phase interface,

where the required oxygen can only be supplied from the analyte solution. The low oxygen concentration and slow oxygen diffusion rate in the liquid limit the enzyme kinetics and the performance of the two-phase electrode. In our previous experimental work,<sup>9–15</sup> this limitation has been addressed by designing enzyme electrodes with a solid-liquid-gas three-phase interface.<sup>16–19</sup> In the three-phase enzyme electrode, the oxygen can be directly and rapidly supplied from the gas phase, which successfully enhances and stabilizes the enzyme kinetics.

Very recently, a novel model was also developed for the three-phase enzymatic system based on glucose oxidase (GOx).<sup>20</sup> It described the interphase (oxygen dissolution) and intraphase (species diffusion) mass transfer, and the homogeneous enzymatic reaction within the system. The quantitative relationship between the interfacial architectures and enzyme kinetics was revealed. It also enabled us to understand the underlying mechanisms that control enzyme kinetics and identify effective design strategies that can boost enzyme kinetics.

The parameters of the interfacial architectures (the structural parameters of the porous substrate and the enzyme-matrix (E-matrix) parameters) affect both enzymatic and electrochemical reactions. The enzymatic reaction occurs throughout the whole E-matrix, but the electrochemical reaction only takes place at the electrode surface. It should be noted that the  $\text{H}_2\text{O}_2$  generated by the enzymatic reaction must diffuse to the electrode surface for the electrochemical reaction. Only part of the  $\text{H}_2\text{O}_2$  can diffuse to the electrode surface and undergo an electrochemical reaction, while the rest escapes into the solution. The electrode interfacial architectures affect the mass transfer of oxygen in the electrode and the production rate of  $\text{H}_2\text{O}_2$ , as well as the diffusion distance of  $\text{H}_2\text{O}_2$  to the electrode surface and the reaction rate of  $\text{H}_2\text{O}_2$ , which finally determines the current generation. It is not possible to directly extrapolate from the effect of the interfacial architectures on enzyme kinetics to its influence on the cascade reactions. Therefore, an in-depth study of the transport phenomena and reaction kinetics within the three-phase enzyme electrode is required to quantitatively correlate the interfacial architectures and the cascade reactions.

In this work, the electrochemical reaction model is incorporated into the previous model to capture the cascade reaction in the three-phase enzyme electrode. Systematic analysis and understanding of the mass transport phenomena and reaction kinetics within this electrode have been performed. This work aims to better understand the effect of the interfacial architectures on the cascade reactions and provide strategies for achieving efficient cascade reactions. The developed model is expected to be an efficient tool for the design of high-performance three-phase enzyme electrodes.

## 2 | MODEL DEVELOPMENT

### 2.1 | System description and model assumptions

As shown in Figure 1, the three-phase enzyme electrode consists of a porous substrate, an electrocatalyst layer, and an E-matrix. The pore size of the substrate is  $d_{\text{pore}}$  and the pore wall thickness of the substrate is  $\delta_{\text{wall}}$ . The porosity of the substrate in the 2D model is defined as  $\epsilon = d_{\text{pore}} / (d_{\text{pore}} + \delta_{\text{wall}})$ . It should be noted that the E-matrix is also a porous media composed of chitosan gel and GOx. The top surface of the substrate is hydrophilic, the rest is hydrophobic. The E-matrix and electrocatalyst are immobilized on the hydrophilic surface of the substrate. When the enzyme electrode is immersed in the electrolyte, the E-matrix can be completely wetted by the liquid phase and becomes a two-phase layer. However, the hydrophobic part of the substrate cannot be wetted and hence forms gas transport channels inside. The solid phase (the E-matrix covered on the substrate), liquid phase (the electrolyte in the E-matrix), and gas phase (the air in the pores of the substrate) hence coexist and form the three-phase interface. The high-concentration oxygen in the gas phase could be rapidly transported to the E-matrix through the three-phase interface.

As shown in Figure 1, the oxygen dissolution occurs at the three-phase interface, and the homogeneous enzymatic reaction occurs

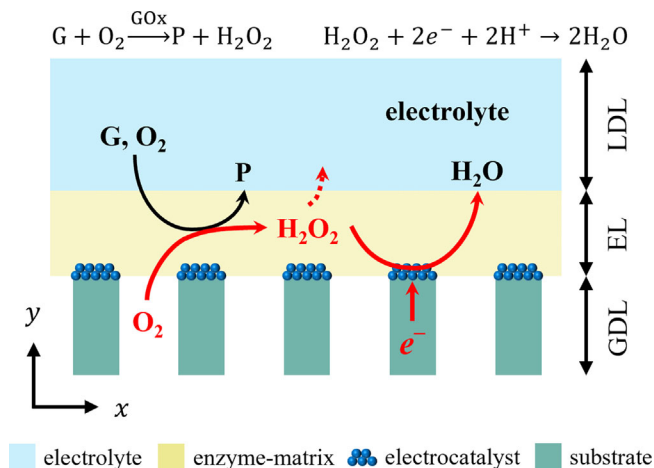


**FIGURE 1** Schematic diagram of the three-phase enzyme electrode based on the GOx showing enzymatic and electrochemical cascade reactions. The electrode consists of three layers, including the liquid diffusion layer (LDL), the enzyme-matrix layer (EL), and the gas diffusion layer (GDL).

within the complete E-matrix. The oxygen ( $\text{O}_2$ ) in the bulk gas is diffused through the porous substrate and dissolved into the liquid phase of the E-matrix. The glucose (G) and oxygen in the bulk liquid are diffused into the E-matrix. In the E-matrix, the oxygen and glucose react with enzyme (E) to produce  $\text{H}_2\text{O}_2$  and by-product (P) in situ. The interface between the pore wall in the porous substrate and the E-matrix is the electrode surface coated with electrocatalysts, while the interface between the pore in the porous substrate and the E-matrix is the non-electrode surface. The heterogeneous electrochemical reaction only occurs on the electrode surface. The part of  $\text{H}_2\text{O}_2$  produced by the enzymatic reaction is consumed on the electrode surface, and the rest is diffused into the electrolyte. The enzymatic and electrochemical reactions form a cascade reaction. Only three species are considered in the model, that is, glucose, oxygen, and  $\text{H}_2\text{O}_2$ .

The three-phase enzyme electrode is modeled at the continuum scale under the steady-state condition. The transport phenomena are only considered in the x and y directions and a 2D model is used (Figure 1). Based on our previous study,<sup>20</sup> the model geometry consists of three layers, including the gas diffusion layer (GDL) formed by the porous substrate, the E-matrix layer (EL), and the liquid diffusion layer (LDL) formed by the electrolyte. Special boundary conditions are specified to couple different layers. The intraphase and interphase mass transfer, the homogeneous enzymatic reaction, and the heterogeneous electrochemical reaction are implemented in the model. The mass transport phenomena in the three layers are described by Fick's law.<sup>21</sup> The oxygen dissolution from the gas phase to the liquid phase is described by Henry's law.<sup>22</sup> Parker<sup>23</sup> found that the Michaelis-Menten approximation works well only with excess oxygen. The enzymatic reaction is hence modeled by ping-pong mechanisms.<sup>24</sup> The current is calculated based on Faraday's and Fick's laws.<sup>25,26</sup> The model implementation details can be found in the [Supporting Information](#).

## 2.2 | Mass transport and homogeneous enzymatic reaction

In the GDL, the governing equation can be written as,

$$-D_{\text{GDL},i} \nabla^2 [i]_g = 0, \quad (1)$$

where  $D_{\text{GDL},i}$  is the effective diffusion coefficient of species  $i$  in the GDL,  $\text{m}^2 \text{s}^{-1}$ ;  $[i]_g$  is the concentration of species  $i$  in the gas phase,  $\text{mol m}^{-3}$ . The symbol  $i$  in the GDL only denotes oxygen since only oxygen in the gas phase participates in the enzymatic reaction. To simulate the mass transfer of oxygen in the porous substrate with pore sizes that are smaller than the mean free path of oxygen, the Knudsen diffusion<sup>20</sup> must be considered in the model. The effective diffusion coefficient of oxygen ( $D_{\text{GDL},\text{O}_2}$ ) is calculated via the Wilke-Bosanquet model,<sup>27</sup>

$$\frac{1}{D_{\text{GDL},\text{O}_2}} = \frac{1}{D_{\text{O}_2}} + \frac{1}{D_{\text{Kn},\text{O}_2}}, \quad (2)$$

where  $D_{\text{O}_2}$  is the molecular diffusion coefficient of oxygen in the free environment,  $\text{m}^2 \text{s}^{-1}$ , which is calculated by an empirical correlation<sup>28</sup>;  $D_{\text{Kn},\text{O}_2}$  is the Knudsen diffusion coefficient of oxygen in the pore,  $\text{m}^2 \text{s}^{-1}$ , which can be calculated based on the kinetics theory,<sup>28</sup>

$$D_{\text{Kn},\text{O}_2} = \frac{d_{\text{pore}}}{3} \sqrt{\frac{8RT}{\pi M_{\text{O}_2}}}, \quad (3)$$

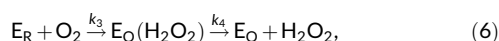
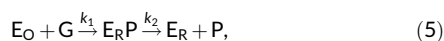
where  $d_{\text{pore}}$  is the pore size,  $\text{m}$ ;  $R$  is the ideal gas constant,  $8.314 \text{ J mol}^{-1} \text{ K}^{-1}$ ;  $T$  is system temperature,  $\text{K}$ ;  $M_{\text{O}_2}$  is the molecular weight of oxygen,  $0.032 \text{ kg mol}^{-1}$ .

In the EL, the homogeneous enzymatic reaction is implemented using the source term in the governing equation. The heterogeneous electrochemical reaction is implemented using specific boundary conditions applied on the electrode surface. The governing equation can be written as,

$$-D_{\text{EL},i} \nabla^2 [i]_l = R_i, \quad (4)$$

where  $D_{\text{EL},i}$  is the diffusion coefficient of species  $i$  in the EL,  $\text{m}^2 \text{s}^{-1}$ ;  $[i]_l$  is the concentration of species  $i$  in the liquid phase,  $\text{mol m}^{-3}$ ;  $R_i$  is the source term of the homogeneous enzymatic reaction,  $\text{mol m}^{-3} \text{s}^{-1}$ ; The symbol  $i$  in the EL denotes three species, that is, glucose, oxygen, and  $\text{H}_2\text{O}_2$ .

The enzymatic kinetics is modeled as the ping-pong mechanism,<sup>29,30</sup> which consists of two sequential reaction steps,



where  $\text{E}_0$  is the oxidized form of GOx;  $\text{E}_\text{R}$  is the reduced form of GOx;  $\text{G}$  is the glucose;  $\text{P}$  is the by-product glucono- $\delta$ -lactone;  $\text{E}_\text{R} \text{P}$  and

$\text{E}_0(\text{H}_2\text{O}_2)$  are two enzyme-product complexes;  $k_1$ ,  $k_2$ ,  $k_3$ , and  $k_4$  are kinetics constants.

It is assumed that the enzymatic reaction reaches a steady state rapidly. The reaction source term can be expressed as,<sup>23</sup>

$$R_i = \pm \frac{\alpha [\text{E}_\text{T}]}{\frac{\beta_\text{G}}{[\text{G}]_l} + \frac{\beta_{\text{O}_2}}{[\text{O}_2]_l} + 1}, \quad (7)$$

where  $\alpha = k_2 k_4 / (k_2 + k_4)$ ;  $\beta_\text{G} = k_2 k_4 / (k_1 (k_2 + k_4))$ ;  $\beta_{\text{O}_2} = (k_2 k_4) / (k_3 (k_2 + k_4))$ ;  $[\text{E}_\text{T}]$  is the total concentration of the active enzyme,  $\text{mol m}^{-3}$ ;  $[\text{G}]_l$  is the glucose concentration in the liquid phase;  $[\text{O}_2]_l$  is the oxygen concentration in the liquid phase. It is assumed that all glucose oxidases are active and uniformly distributed in the EL. Hence,  $[\text{E}_\text{T}]$  remains constant.<sup>31</sup> The kinetics constants provided by Atkinson and Lester<sup>29,30</sup> are used. The positive value of the  $R_i$  represents the production rate of  $\text{H}_2\text{O}_2$ , and the negative value represents the consumption rate of glucose or oxygen.

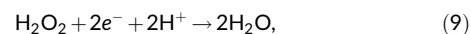
In the LDL, the governing equation can be written as,

$$-D_{\text{LDL},i} \nabla^2 [i]_l = 0, \quad (8)$$

where  $D_{\text{LDL},i}$  is the diffusion coefficient of species  $i$  in the LDL,  $\text{m}^2 \text{s}^{-1}$ ; The symbol  $i$  in LDL also denotes three species, that is, glucose, oxygen, and  $\text{H}_2\text{O}_2$ .

## 2.3 | Heterogeneous electrochemical reaction

The  $\text{H}_2\text{O}_2$  is reduced on the electrode surface by the action of the electrocatalyst, and the reduction current is generated at the same time. The mechanism of electrochemical reduction of  $\text{H}_2\text{O}_2$  is,



where  $\text{e}^-$  is transported by the porous substrate (see Figure 1);  $\text{H}^+$  is provided by the electrolyte.

The electrode surface is imposed with specific boundary conditions to simulate the heterogeneous electrochemical reaction. On the electrode surface, glucose and oxygen do not participate in the electrochemical reaction. Hence, zero-flux boundary conditions are applied to them. However, the  $\text{H}_2\text{O}_2$  will be consumed under the electrochemical reaction. In the experiment, the electrochemical reaction rate can reach a peak value by adjusting the experimental parameters (e.g., the overpotential, the amount of electrocatalyst). Hence, for a diffusion-controlled process, the  $\text{H}_2\text{O}_2$  concentration on the electrode surface is assumed to be zero. The heterogeneous electrochemical reaction is implemented by following boundary conditions,

$$\begin{cases} -\mathbf{n} \cdot (-D_{\text{EL},\text{G}} \nabla [\text{G}]_l) = 0 \\ -\mathbf{n} \cdot (-D_{\text{EL},\text{O}_2} \nabla [\text{O}_2]_l) = 0, \\ [\text{H}_2\text{O}_2]_l = 0 \end{cases} \quad (10)$$

where  $D_{\text{ELG}}$  is the diffusion coefficient of glucose in the EL,  $\text{m}^2 \text{s}^{-1}$ ;  $D_{\text{EL},\text{O}_2}$  is the diffusion coefficient of oxygen in the EL,  $\text{m}^2 \text{s}^{-1}$ ;  $[\text{H}_2\text{O}_2]_{\text{l}}$  is the  $\text{H}_2\text{O}_2$  concentration in the liquid phase,  $\text{mol m}^{-3}$ .

The current density on the electrode surface depends upon the  $\text{H}_2\text{O}_2$  flux across the electrode surface. The current density is calculated by,

$$j = nFJ_{\text{H}_2\text{O}_2}, \quad (11)$$

where  $j$  is the current density,  $\text{A m}^{-2}$ ;  $n$  is the stoichiometric number of electrons for an electrochemical reaction,<sup>25</sup>  $n = 2$ ;  $F$  is the Faraday constant,  $96485 \text{ C mol}^{-1}$ ;  $J_{\text{H}_2\text{O}_2}$  is the  $\text{H}_2\text{O}_2$  flux caused by the electrochemical reaction on the electrode surface,  $\text{mol m}^{-2} \text{s}^{-1}$ .

The current is related to the mean current density and the electrochemical reaction area,

$$i = \bar{j} \cdot A_{\text{e}}, \quad (12)$$

where  $i$  is the current, A;  $\bar{j}$  is the mean current density,  $\text{A m}^{-2}$ ;  $A_{\text{e}}$  is the electrochemical reaction area,  $\text{m}^2$ , which is related to the porosity,

$$A_{\text{e}} = (1 - \epsilon)A_{\text{total}}, \quad (13)$$

where  $A_{\text{total}}$  is the total area between the porous substrate and the EL. In this study,  $A_{\text{total}} = 0.2 \text{ cm}^2$ .

All model parameters are listed in Table S1. The boundary conditions and initial conditions can be found in the Supporting Information.

### 3 | RESULTS AND DISCUSSION

In a three-phase enzyme electrode, the current generation can be influenced by multiple factors. As mentioned earlier, the enzymatic reaction generates  $\text{H}_2\text{O}_2$ , and then part of  $\text{H}_2\text{O}_2$  diffuses to the electrode surface to be consumed by the electrochemical reaction, while the rest escapes into the solution. Therefore, both the production rate and escape rate of  $\text{H}_2\text{O}_2$  determine the reaction rate of  $\text{H}_2\text{O}_2$ , which consequently affects the current generation.

Among the parameters of the interfacial architectures, both the structural parameters of the porous substrate (porosity  $\epsilon$  and pore size  $d_{\text{pore}}$ ) and the E-matrix parameters (EL thickness  $\delta_{\text{EL}}$  and enzyme concentration  $[\text{E}_T]$ ) can affect enzymatic and electrochemical cascade reactions. The effect of each parameter on the current generation will be discussed separately.

#### 3.1 | Effect of the porosity of the substrate

Figure 2 shows the effect of the porosity on the three-phase enzyme electrode. The porosities range from 0.05 to 0.95, whose influences on current generation are investigated under the conditions of two pore wall thicknesses, specifically  $\delta_{\text{wall}} = 10$  and  $1000 \text{ nm}$ . The other parameters are  $\delta_{\text{EL}} = 1 \mu\text{m}$ , and  $[\text{E}_T] = 1 \text{ mol m}^{-3}$ .

Figure 2A shows the results for the cases with  $\delta_{\text{wall}} = 10 \text{ nm}$ . It can be observed in Figure 2A1 that the current decreases with increasing porosity, yet remains substantially high. It should be noted

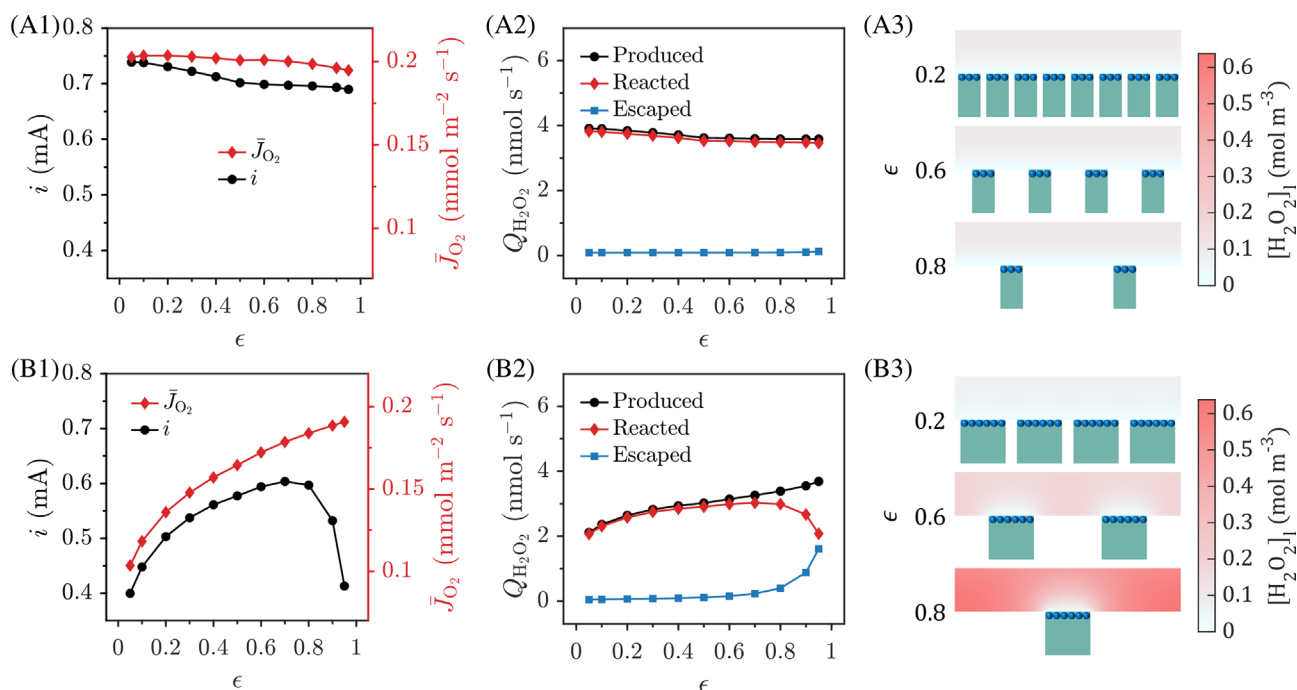


**FIGURE 2** Effect of the porosity on the three-phase enzyme electrode. (A) The results for the case of  $\delta_{\text{wall}} = 10 \text{ nm}$ . (B) The results for the case of  $\delta_{\text{wall}} = 1000 \text{ nm}$ . (A1) and (B1) show the current ( $i$ ) and the supply rate of oxygen ( $\bar{J}_{\text{O}_2}$ ) under different porosities. (A2) and (B2) show the rates of production, reaction, and escape ( $Q_{\text{H}_2\text{O}_2}$ ) of  $\text{H}_2\text{O}_2$  under different porosities. (A3) and (B3) show the  $\text{H}_2\text{O}_2$  concentration ( $[\text{H}_2\text{O}_2]_{\text{l}}$ ) distribution in the EL, where porosities are  $\epsilon = 0.2, 0.6$ , and  $0.8$ , respectively. The dimensions of (A3) and (B3) are not to scale.

that the current is directly determined by the reaction rate of  $\text{H}_2\text{O}_2$ . To better explain this trend in current, the production rate, reaction rate, and escape rate of  $\text{H}_2\text{O}_2$  within the electrode were plotted and analyzed, where the production rate of  $\text{H}_2\text{O}_2$  equals the sum of the reaction rate and escape rate of  $\text{H}_2\text{O}_2$ .

As shown in Figure 2A2, the production rate of  $\text{H}_2\text{O}_2$  remains high regardless of the porosity. Since the previous study<sup>20</sup> confirmed that the supply rate of oxygen dominantly determines the production rate of  $\text{H}_2\text{O}_2$ , this high production rate can be attributed to the fact that the supply rate of oxygen is sufficiently large (see Figure 2A1). Furthermore, the supply rate of oxygen is related to the structure of the porous substrate. As shown in Figure 3A1, the EL coated on the porous substrate can be divided into two types of regions. The different types of regions have been separated by gray dashed lines. Specifically, one type of region is adjacent to the pore (e.g., region A), while the other type of region is adjacent to the pore wall (e.g., region B). It can be observed that region A is closer to the pore than region B. Therefore, region B has greater difficulty in obtaining oxygen from the pore than region A. In other words, compared to the enzymatic reaction in region A, the enzymatic reaction in region B is more prone to be limited by the mass transfer of oxygen. As the pore wall thickness decreases (see Figure 3A2), the mean diffusion distance and time of oxygen to diffuse from the pore to region B also decrease. This facilitates the mass transfer of oxygen in the EL, thus increasing the supply rate of oxygen. Consequently, the production rate of  $\text{H}_2\text{O}_2$  increases with decreasing pore wall thickness. In this case, since the pore wall is thin enough ( $\delta_{\text{wall}} = 10\text{ nm}$ ), both the supply rate of oxygen and the production rate of  $\text{H}_2\text{O}_2$  stay at a high level regardless of the porosity.

As shown in Figure 2A2, regardless of the porosity, nearly all  $\text{H}_2\text{O}_2$  is consumed and only a negligible amount escapes from the EL. This is related to the mass transfer process of the  $\text{H}_2\text{O}_2$  at different regions within the EL. It should be noted that the  $\text{H}_2\text{O}_2$  can only be consumed at the electrode surface on the pore wall. As shown in Figure 3B1, the  $\text{H}_2\text{O}_2$  generated at region A needs to travel a longer distance to reach the electrode surface than that generated at region B. Therefore, the electrochemical reaction is prone to be limited by the mass transfer of  $\text{H}_2\text{O}_2$ . As the pore size gets smaller (see Figure 3B2), the mean diffusion distance and time of  $\text{H}_2\text{O}_2$  to diffuse from region A to the electrode surface also decrease. This facilitates the mass transfer of the  $\text{H}_2\text{O}_2$  from region A to the electrode surface, thus more  $\text{H}_2\text{O}_2$  can be consumed and less  $\text{H}_2\text{O}_2$  can escape from the EL. In other words, the reaction rate of  $\text{H}_2\text{O}_2$  increases, and the escape rate of  $\text{H}_2\text{O}_2$  decreases as the pore size gets smaller. In the case of  $\delta_{\text{wall}} = 10\text{ nm}$ , the pore size ranges from  $d_{\text{pore}} = 0.526$  to  $190\text{ nm}$  as porosity changes from  $\epsilon = 0.05$  to  $0.95$ . These pore sizes are small enough, therefore the reaction rate of  $\text{H}_2\text{O}_2$  and current stay high, while the escape rate of  $\text{H}_2\text{O}_2$  stays low. To visualize the  $\text{H}_2\text{O}_2$  concentration distributions in the EL, Figure 2A3 was plotted. It can be observed that the  $\text{H}_2\text{O}_2$  concentration in the EL stays low regardless of the porosity. This further confirms that most  $\text{H}_2\text{O}_2$  is consumed, thus the escape rate of  $\text{H}_2\text{O}_2$  is negligible. Consequently, the reaction rate of  $\text{H}_2\text{O}_2$  remains at a large value, leading to a consistently high current.

Figure 2B shows the results for the case of  $\delta_{\text{wall}} = 1000\text{ nm}$ . Unlike the case of  $\delta_{\text{wall}} = 10\text{ nm}$ , Figure 2B1 shows that the current first increases and then decreases with increasing porosity. The peak

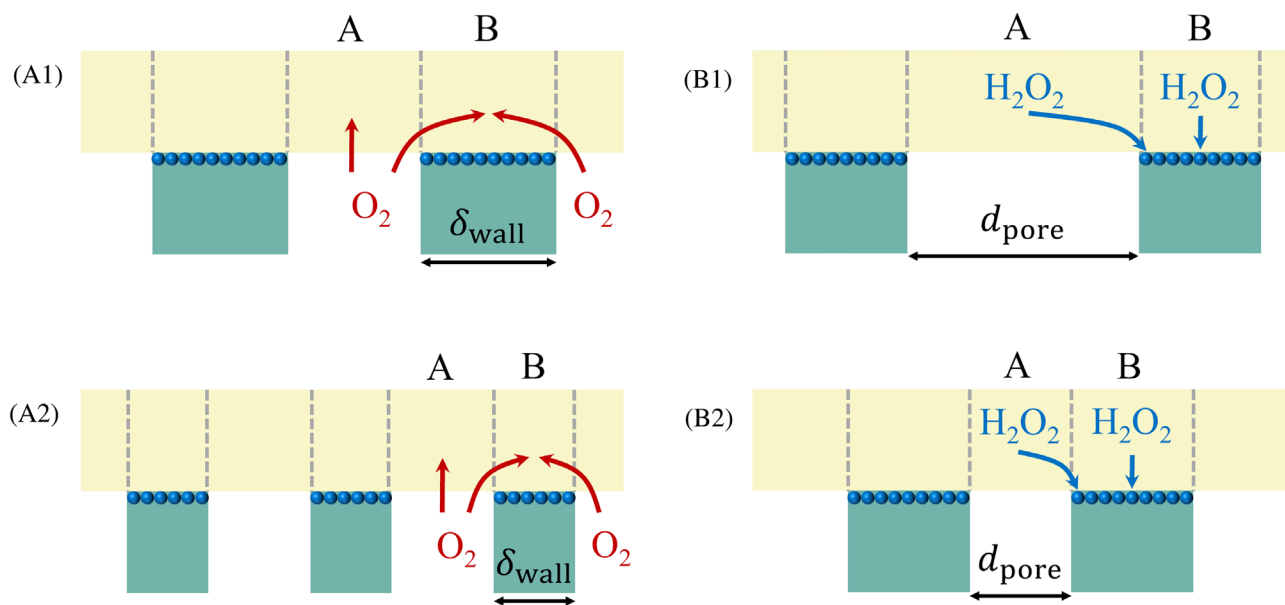


**FIGURE 3** Diagram of diffusion pathway of the oxygen and  $\text{H}_2\text{O}_2$  at different regions within the EL. Region A is adjacent to the pore. Region B is adjacent to the pore wall. (A) Compared with region A, region B is more difficult to obtain oxygen from the gas phase. As the pore wall thickness decreases, the mean diffusion distance and time of oxygen to diffuse from the gas phase to region B also decrease. This facilitates the mass transfer of oxygen in the EL. (B) Compared with the  $\text{H}_2\text{O}_2$  generated at region B, the  $\text{H}_2\text{O}_2$  generated at region A is more difficult to be consumed by the electrochemical reaction. As the pore size decreases, the mean diffusion distance and time of  $\text{H}_2\text{O}_2$  to diffuse from region A to the electrocatalyst surface also decrease. This facilitates the mass transfer of the  $\text{H}_2\text{O}_2$  from region A to the electrode surface.

value of the current can be observed at around  $\epsilon = 0.7$ . The current is smaller compared to the case of  $\delta_{\text{wall}} = 10 \text{ nm}$  regardless of porosity. As shown in Figure 2B2, the production rate of  $\text{H}_2\text{O}_2$  continuously increases with increasing porosity. This is because the pore wall is too thick ( $\delta_{\text{wall}} = 1000 \text{ nm}$ ), impeding the mass transfer of oxygen. In addition, in the case of low porosity, the hypoxic region (i.e., region B) is large (see the case of  $\epsilon = 0.2$  in Figure 2B3). However, this region gradually decreases with the porosity (see the case of  $\epsilon = 0.8$  in Figure 2B3), resulting in the more efficient mass transfer of oxygen in the EL. This finally leads to a continuous increase in the supply rate of oxygen (see Figure 2B1) as porosity increases, which finally leads to a continuous increase in the production rate of  $\text{H}_2\text{O}_2$ . This phenomenon has been confirmed in the previous study.<sup>20</sup> In addition, the escape rate of  $\text{H}_2\text{O}_2$  also increases with increasing porosity. This is because the pore size increases with increasing porosity when the pore wall thickness is fixed. As shown in Figure 2B2, the reaction rate of  $\text{H}_2\text{O}_2$  is lower than the case of  $\delta_{\text{wall}} = 10 \text{ nm}$  regardless of porosity, thus the current is lower than that case. It can also be found that the reaction rate of  $\text{H}_2\text{O}_2$  stays at a low level for both too-low and too-high porosity. This is related to the variation of the production rate and escape rate of  $\text{H}_2\text{O}_2$ . When the porosity is small (e.g.,  $\epsilon = 0.2$ ), the supply rate of oxygen (see Figure 2B1) is limited, thereby limiting the production rate of  $\text{H}_2\text{O}_2$  (see Figure 2B2). In addition, in that case, the pore size is small ( $d_{\text{pore}} = 250 \text{ nm}$ ), most  $\text{H}_2\text{O}_2$  is consumed (see the case of  $\epsilon = 0.2$  in Figure 2B3) and the escape rate of  $\text{H}_2\text{O}_2$  is negligible. However, there is insufficient  $\text{H}_2\text{O}_2$  production. This finally leads to a small reaction rate of  $\text{H}_2\text{O}_2$  and a low current. When the porosity is large (e.g.,  $\epsilon = 0.8$ ), the supply rate of oxygen is large (see Figure 2B1), therefore enabling a large production rate of  $\text{H}_2\text{O}_2$ . However, the pore size becomes excessively large in such a case ( $d_{\text{pore}} = 4000 \text{ nm}$ ), which limits the reaction rate of  $\text{H}_2\text{O}_2$  (see the case of  $\epsilon = 0.8$  in Figure 2B3) and enhances the escape rate of  $\text{H}_2\text{O}_2$ . This also finally leads to a small reaction rate of  $\text{H}_2\text{O}_2$  and a low current. When the porosity is between the above two values (e.g.,  $\epsilon = 0.6$ ), the production rate of  $\text{H}_2\text{O}_2$  is relatively large and the escape rate of  $\text{H}_2\text{O}_2$  is relatively small, hence the reaction rate of  $\text{H}_2\text{O}_2$  and the current can be maintained at a relatively

high level. In addition, when the porosity is 0.9, the pore size is  $9 \mu\text{m}$ , and the escape rate of  $\text{H}_2\text{O}_2$  accounts for about 24.9% of the production rate of  $\text{H}_2\text{O}_2$ . The previous experiment<sup>32</sup> confirmed that, for the pore size of around  $10 \mu\text{m}$ , the escape rate accounts for about 20% of the production rate. The escape rates in the experimental and simulation systems are similar, which justifies the accuracy of the model.

### 3.2 | Effect of the pore size of the substrate

Figure 4 shows the effect of the pore size on the three-phase enzyme electrode. The pore sizes range from 2 to  $10,000 \text{ nm}$ . The other parameters are  $\epsilon = 0.5$ ,  $\delta_{\text{EL}} = 1 \mu\text{m}$ , and  $[E_T] = 1 \text{ mol m}^{-3}$ .

As shown in Figure 4A, the current first increases and eventually reaches a plateau as the pore size decreases. Similar trends can also be observed for the production rate of  $\text{H}_2\text{O}_2$  from Figure 4B. In the case of constant porosity, the pore wall thickness decreases with decreasing the pore size (in the case of  $d_{\text{pore}} = 10,000, 1000$ , and  $10 \text{ nm}$ ,  $\delta_{\text{wall}} = 10,000, 1000$ , and  $10 \text{ nm}$ ), thus the supply rate of oxygen increases (see Figure 4A). Consequently, the production rate of  $\text{H}_2\text{O}_2$  increases. However, a sufficiently thin pore wall significantly reduces the mean diffusion distance and time of oxygen from the pore to region B (see Figure 3A). This also results in a significant decrease in the difference in the mass transfer of oxygen between regions A and B. Consequently, the EL is no longer hypoxic. This implies that the supply rate of oxygen and the production rate of  $\text{H}_2\text{O}_2$  gradually reach a maximal limit as the pore size decreases. As shown in Figure 4B, the escape rate of  $\text{H}_2\text{O}_2$  decreases with decreasing the pore size. This phenomenon is consistent with the mechanism mentioned in Figure 3B. Figure 4C shows the mean  $\text{H}_2\text{O}_2$  concentration inside the EL decreases with decreasing the pore size. This further confirms that as the pore size decreases, more  $\text{H}_2\text{O}_2$  is consumed and less  $\text{H}_2\text{O}_2$  can escape. Therefore, the reaction rate of  $\text{H}_2\text{O}_2$  and the current increase with decreasing the pore size. In other words, decreasing the pore size when the porosity is fixed facilitates both the mass transfer of oxygen and  $\text{H}_2\text{O}_2$  in the cascade reactions.

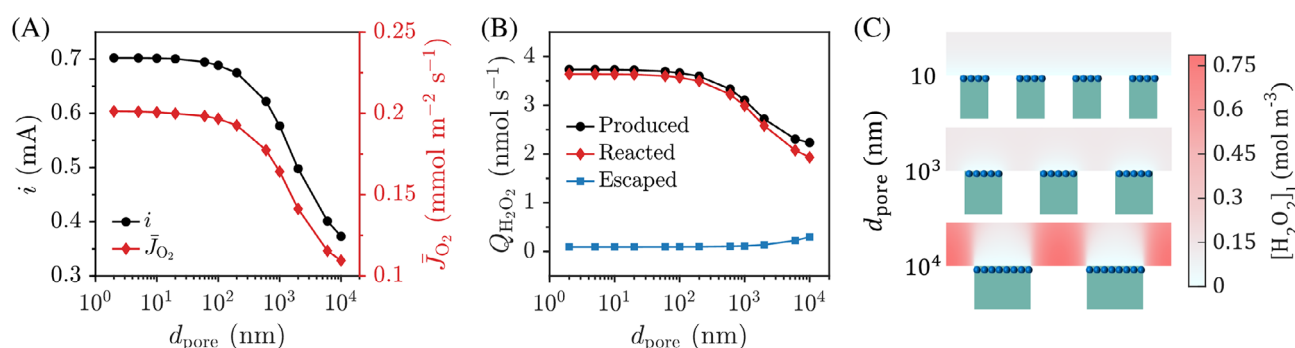


**FIGURE 4** Effect of pore size on the three-phase enzyme electrode. (A)  $i$  and  $\bar{J}_{\text{O}_2}$  under different pore sizes. (B)  $Q_{\text{H}_2\text{O}_2}$  under different pore sizes. (C)  $[\text{H}_2\text{O}_2]$  distribution in the EL, where pore sizes are  $d_{\text{pore}} = 10 \text{ nm}$ ,  $1000 \text{ nm}$ , and  $10,000 \text{ nm}$ , respectively. It should be noted that the dimensions of pores are not to scale.



This increases the production rate of  $\text{H}_2\text{O}_2$  and decreases the escape rate of  $\text{H}_2\text{O}_2$ , hence increasing the current.

### 3.3 | Effect of the enzyme-matrix layer thickness

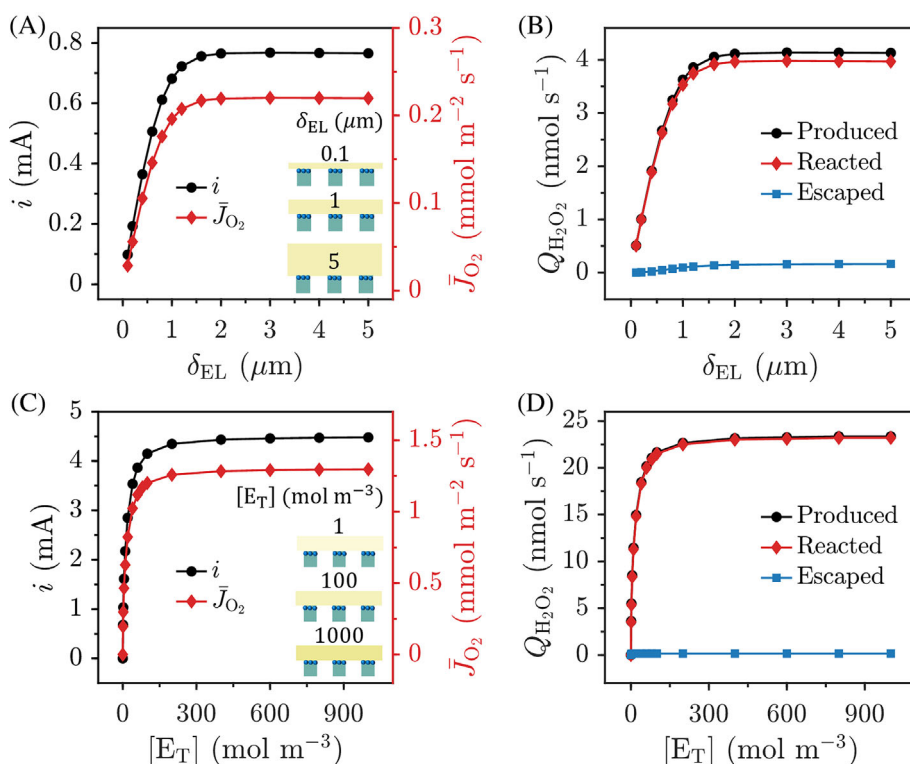
Figure 5A, B shows the effect of the EL thickness on the three-phase enzyme electrode. The EL thicknesses range from 0.1 to 5  $\mu\text{m}$ . The other parameters are fixed at  $\epsilon = 0.5$ ,  $d_{\text{pore}} = 100 \text{ nm}$ , and  $[\text{E}_\text{T}] = 1 \text{ mol m}^{-3}$ . As shown in Figure 5A, when the EL is thin (e.g.,  $\delta_{\text{EL}} \leq 1.5 \mu\text{m}$ ), the current increases rapidly with increasing the EL thickness. However, when the EL is thick (e.g.,  $1.5 \mu\text{m} \leq \delta_{\text{EL}} \leq 5 \mu\text{m}$ ), the current barely changes even if the EL thickness is further increased.

As shown in Figure 5B, the production rate of  $\text{H}_2\text{O}_2$  increases rapidly when the EL is thin (e.g.,  $\delta_{\text{EL}} \leq 1.5 \mu\text{m}$ ). As confirmed in the previous study, this is because there is sufficient oxygen within the EL. Increasing the EL thickness allows more oxygen to participate in the enzymatic reaction (see Figure 5A), thus increasing the production rate of  $\text{H}_2\text{O}_2$ . However, an excessively thick EL (e.g.,  $1.5 \mu\text{m} \leq \delta_{\text{EL}} \leq 5 \mu\text{m}$ ) increases the mean diffusion distance and time of oxygen to diffuse into the EL, leading to hypoxia in the EL far from the three-phase interface (see Figure 51b). Consequently, the production rate of  $\text{H}_2\text{O}_2$  scarcely increases further. This implies that a thicker EL promotes oxygen utilization but impedes the mass transfer of oxygen, which eventually limits the production rate of  $\text{H}_2\text{O}_2$ . Furthermore, the escape rate of  $\text{H}_2\text{O}_2$  is always small since the pore size is small and constant ( $d_{\text{pore}} = 100 \text{ nm}$ ). Therefore, the reaction rate of  $\text{H}_2\text{O}_2$  and the current are almost determined by the production rate of  $\text{H}_2\text{O}_2$ .

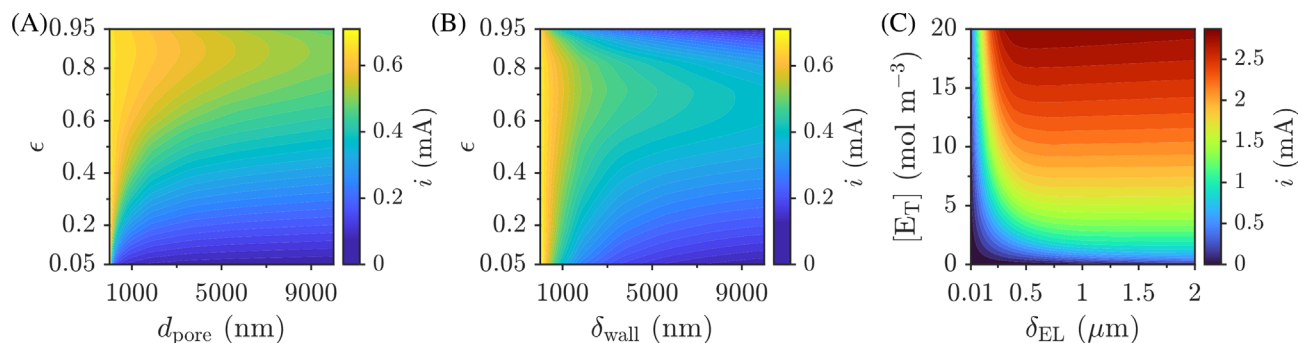
### 3.4 | Effect of the enzyme concentration

Figure 5C, D shows the effect of the enzyme concentration on the three-phase enzyme electrode. The enzyme concentrations range from 0.001 to 1000  $\text{mol m}^{-3}$ . The other parameters are fixed at  $\epsilon = 0.5$ ,  $d_{\text{pore}} = 100 \text{ nm}$ , and  $\delta_{\text{EL}} = 1 \mu\text{m}$ . As shown in Figure 5C, similar to the effect of the EL thickness, the current increases rapidly with increasing the enzyme concentration when the enzyme concentration is low (e.g.,  $[\text{E}_\text{T}] \leq 150 \text{ mol m}^{-3}$ ). However, at high enzyme concentrations (e.g.,  $150 \text{ mol m}^{-3} \leq [\text{E}_\text{T}] \leq 1000 \text{ mol m}^{-3}$ ), the current hardly changes even if the enzyme concentration is further increased.

As shown in Figure 5D, the production rate of  $\text{H}_2\text{O}_2$  increases rapidly at low enzyme concentrations (e.g.,  $[\text{E}_\text{T}] \leq 150 \text{ mol m}^{-3}$ ). As confirmed in the previous study, this is because there is sufficient oxygen within the EL (see Figure 51c). Increasing the enzyme concentration allows more oxygen to participate in the enzymatic reaction (see Figure 5C), thus increasing the production rate of  $\text{H}_2\text{O}_2$ . However, increasing the enzyme concentration also increases the reaction rate of oxygen (see Equation (7)). This eventually causes hypoxia in the EL away from the three-phase interface (see Figure 51c) at high enzyme concentrations (e.g.,  $150 \text{ mol m}^{-3} \leq [\text{E}_\text{T}] \leq 1000 \text{ mol m}^{-3}$ ). Consequently, the production rate of  $\text{H}_2\text{O}_2$  barely increases further. This implies that at high enzyme concentrations, the reaction rate of oxygen increases, but the mass transfer of oxygen remains relatively stable, which eventually limits the supply rate of oxygen and the production rate of  $\text{H}_2\text{O}_2$ . Similar to the effect of EL thickness, the escape rate of  $\text{H}_2\text{O}_2$  stays at a low level since the pore size is small and constant ( $d_{\text{pore}} = 100 \text{ nm}$ ). Therefore, the reaction rate of  $\text{H}_2\text{O}_2$  and the current are almost determined by the production rate of  $\text{H}_2\text{O}_2$ .



**FIGURE 5** Effect of EL thickness and enzyme concentration on the three-phase enzyme electrode. (A)  $i$  and  $\bar{J}_{\text{O}_2}$  under different EL thicknesses. (B)  $Q_{\text{H}_2\text{O}_2}$  under different EL thicknesses. (C)  $i$  and  $\bar{J}_{\text{O}_2}$  under different enzyme concentrations. (D)  $Q_{\text{H}_2\text{O}_2}$  under different enzyme concentrations.



**FIGURE 6** Effect of multiple parameters on the three-phase enzyme electrode. (A) Effect of  $d_{\text{pore}}$  and  $\epsilon$  on the current when  $\delta_{\text{EL}} = 1 \mu\text{m}$  and  $[E_T] = 1 \text{ mol m}^{-3}$ . (B) Effect of  $\delta_{\text{wall}}$  and  $\epsilon$  on the current when  $\delta_{\text{EL}} = 1 \mu\text{m}$  and  $[E_T] = 1 \text{ mol m}^{-3}$ . (C) Effect of  $\delta_{\text{EL}}$  and  $[E_T]$  on the current when  $d_{\text{pore}} = 100 \text{ nm}$  and  $\epsilon = 0.5$ .

### 3.5 | Effect of multiple parameters

After analyzing the effect of individual parameters, the joint effect of multiple parameters is analyzed further. Figure 6A shows the effect of pore size and porosity on the current for a fixed EL thickness and enzyme concentration. The pore sizes range from 2 to 10,000 nm. The porosities range from 0.05 to 0.95. It can be observed that in the case of the same pore size, electrodes with higher porosities (e.g.,  $\epsilon \geq 0.7$ ) tend to generate relatively higher currents. This is because when the pore size is constant, the pore wall thickness decreases with increasing porosity. This enhances the production rate of  $\text{H}_2\text{O}_2$  but hardly affects the escape rate of  $\text{H}_2\text{O}_2$ . In the case of the same porosity, electrodes with smaller pore sizes always generate relatively higher currents. As discussed earlier, this is because decreasing the pore size at the same porosity also decreases the pore wall thickness, which simultaneously increases the production rate of  $\text{H}_2\text{O}_2$  and decreases the escape rate of  $\text{H}_2\text{O}_2$ . Consequently, the reaction rate of  $\text{H}_2\text{O}_2$  and the current increase.

In certain special cases (e.g., when the porous substrate possesses a mesh structure or a wire structure), however, the pore wall thickness may be more readily measured than the pore size. Consequently, the effect of pore wall thickness and porosity on current was also explored for a fixed EL thickness and enzyme concentration, as shown in Figure 6B. The pore wall thicknesses range from 2 to 10,000 nm. The porosities range from 0.05 to 0.95. It can be observed that for thin pore walls, electrodes with any porosity ( $0.05 \leq \epsilon \leq 0.95$ ) can obtain a relatively high current. However, for thick pore walls, electrodes with high porosity (e.g.,  $0.6 \leq \epsilon \leq 0.8$ ) should be prepared to obtain a maximum current. The reasons for this complex phenomenon are twofold. On the one hand, both the pore wall thickness and the pore size range widely ( $2 \text{ nm} \leq \delta_{\text{wall}} \leq 10,000 \text{ nm}$  and  $0.105 \text{ nm} \leq d_{\text{pore}} \leq 190,000 \text{ nm}$ ) in this case, which leads to substantial fluctuation in both the production rate and escape rate of  $\text{H}_2\text{O}_2$ . On the other hand, the escape and reaction of  $\text{H}_2\text{O}_2$  compete with each other. This finally results in a complex pattern of variations in the current. Additionally, in the case of the same porosity, electrodes with thinner pore walls always generate relatively higher currents. This is because decreasing the pore wall thickness at the same porosity also decreases the pore size, which

simultaneously increases the production rate of  $\text{H}_2\text{O}_2$  and decreases the escape rate of  $\text{H}_2\text{O}_2$ . Consequently, the reaction rate of  $\text{H}_2\text{O}_2$  and the current increase.

Figure 6C shows the effect of EL thickness and enzyme concentration on current for a fixed porosity and pore size. The EL thicknesses range from 0.01 to 2  $\mu\text{m}$ . The enzyme concentrations range from 0.001 to 20  $\text{mol m}^{-3}$ . The other parameters are fixed at  $\epsilon = 0.5$  and  $d_{\text{pore}} = 100 \text{ nm}$ . It can be found that if the enzyme concentration and the EL thickness reach a certain value (e.g.,  $[E_T] \geq 5 \text{ mol m}^{-3}$  and  $\delta_{\text{EL}} \geq 0.5 \mu\text{m}$ ), the current scarcely varies with increasing the EL thickness but increases rapidly with increasing enzyme concentration. Since the EL parameters have little effect on the escape rate of  $\text{H}_2\text{O}_2$  in this case, the current is almost determined by the production rate of  $\text{H}_2\text{O}_2$ . In other words, the effects of the EL thickness and enzyme concentration on the current are almost consistent with their effects on the production rate of  $\text{H}_2\text{O}_2$  (see the previous study<sup>20</sup>).

In summary, the optimal structural parameters of the porous substrate and the EL parameters for maximizing the current can be identified from Figure 6.

## 4 | CONCLUSIONS

In summary, this work developed a mathematical model for capturing cascade reaction kinetics at the three-phase interface enzyme electrode. Numerical simulation was conducted to investigate the effect of the interfacial architectures on the performance of cascade reactions in the three-phase enzyme electrode. Four structural parameters of the electrode were investigated, including the porosity, the pore wall thickness, the EL thickness, and the enzyme concentration. Key findings are summarized below.

1. Beyond the efficiency of the enzymatic reaction, the efficiency of the electrochemical reaction also plays an important role in enhancing the current generation.
2. The key factors influencing the electrode performance are the mass transfer of oxygen and  $\text{H}_2\text{O}_2$ . Efficient mass transfer is beneficial to the cascade reactions, which can increase the production



rate of  $\text{H}_2\text{O}_2$  and decrease the escape rate of  $\text{H}_2\text{O}_2$ , hence enhancing the current generation.

- Decreasing the pore wall thickness facilitates the mass transfer of oxygen, which is beneficial to the enzymatic reaction. Consequently, the supply rate of oxygen and the production rate of  $\text{H}_2\text{O}_2$  increase. However, the supply rate of oxygen and the production rate of  $\text{H}_2\text{O}_2$  can reach a plateau in cases with excessively thin pore walls.
- Decreasing the pore size facilitates the mass transfer of  $\text{H}_2\text{O}_2$ , which is beneficial to the electrochemical reaction. Consequently, the reaction rate of  $\text{H}_2\text{O}_2$  increases and the escape rate of  $\text{H}_2\text{O}_2$  decreases.
- Increasing the porosity facilitates the mass transfer of oxygen, hence increasing the supply rate of oxygen and the production rate of  $\text{H}_2\text{O}_2$ .
- Increasing the EL thickness and enzyme concentration increases the production rate of  $\text{H}_2\text{O}_2$ . However, an excessively thick EL impedes the mass transfer of oxygen in the EL, and an excessively high enzyme concentration enhances the reaction rate of oxygen. Consequently, the supply rate of oxygen and the production rate of  $\text{H}_2\text{O}_2$  are finally limited and reach a plateau.
- For a specific substrate structure, the EL thickness and the enzyme concentration have less effect on the escape rate of  $\text{H}_2\text{O}_2$ , and the current generation is mainly controlled by the production rate of  $\text{H}_2\text{O}_2$ .

By resorting to the new model, we have gained an in-depth understanding of how the three-phase interfacial architecture can influence both enzymatic and succeeding electrochemical reactions, which lays a theoretical foundation for achieving an efficient cascade reaction. This model should be an effective and promising tool for the design of high-performance three-phase enzyme electrodes that can potentially be used in disease diagnosis and health monitoring.

## AUTHOR CONTRIBUTIONS

**Siyu Zou:** Formal analysis (equal); investigation (lead); methodology (equal); software (lead); writing – original draft (lead); writing – review and editing (equal). **Jie Xiao:** Conceptualization (equal); formal analysis (equal); methodology (equal); supervision (equal); writing – review and editing (equal). **Xinjian Feng:** Conceptualization (lead); formal analysis (equal); funding acquisition (lead); methodology (equal); supervision (equal); writing – review and editing (equal).

## ACKNOWLEDGMENTS

This work was supported by the National Key Research and Development Program of China (2019YFA0709200), the National Natural Science Foundation of China (21988102, 21978184), the Jiangsu Funding Program for Excellent Postdoctoral Talent, the Priority Academic Program Development of Jiangsu Higher Education Institutions (PAPD), and the Project of Scientific and Technologic Infrastructure of Suzhou (SZS201905). Prof. Jie Xiao acknowledges the “Jiangsu Innovation and Entrepreneurship (Shuang Chuang) Program” and the “Jiangsu Specially-Appointed Professors Program”.

## DATA AVAILABILITY STATEMENT

All data required to evaluate the conclusions in this paper are present in the paper itself and the [Supporting Information](#). Additional data that support the findings of this study are available from the corresponding author upon reasonable request.

## ORCID

Siyu Zou  <https://orcid.org/0000-0002-9152-9844>

Jie Xiao  <https://orcid.org/0000-0001-7842-7862>

Xinjian Feng  <https://orcid.org/0000-0002-3646-9199>

## REFERENCES

- Yang Y, Song Y, Bo X, et al. A laser-engraved wearable sensor for sensitive detection of uric acid and tyrosine in sweat. *Nat Biotechnol*. 2020;38(2):217–224.
- He W, Wang C, Wang H, et al. Integrated textile sensor patch for real-time and multiplex sweat analysis. *Sci Adv*. 2019;5(11):eaax0649.
- Abate-Shen C, Shen MM. The prostate-cancer metabolome. *Nature*. 2009;457(7231):799–800.
- Kumar V, Kukkar D, Hashemi B, Kim K-H, Deep A. Advanced functional structure-based sensing and imaging strategies for cancer detection: possibilities, opportunities, challenges, and prospects. *Adv Funct Mater*. 2019;29(16):1807859.
- Xu C, Wu F, Yu P, Mao L. In vivo electrochemical sensors for neurochemicals: recent update. *ACS Sens*. 2019;4(12):3102–3118.
- Ye S, Hananya N, Green O, et al. A highly selective and sensitive chemiluminescent probe for real-time monitoring of hydrogen peroxide in cells and animals. *Angew Chem Int Ed*. 2020;59(34):14326–14330.
- Weinstein R, Savariar EN, Felsen CN, Tsien RY. In vivo targeting of hydrogen peroxide by activatable cell-penetrating peptides. *J Am Chem Soc*. 2014;136(3):874–877.
- Teymourian H, Barfidokht A, Wang J. Electrochemical glucose sensors in diabetes management: an updated review (2010–2020). *Chem Soc Rev*. 2020;49(21):7671–7709.
- Mi L, Yu J, He F, et al. Boosting gas involved reactions at nanochannel reactor with joint gas–solid–liquid interfaces and controlled wettability. *J Am Chem Soc*. 2017;139(30):10441–10446.
- Guan F, Zhang J, Tang H, Chen L, Feng X. An enhanced enzymatic reaction using a triphase system based on superhydrophobic mesoporous nanowire arrays. *Nanoscale Horiz*. 2019;4(1):231–235.
- Wang H, Zhang J, Wang D, Wang Z, Chen Y, Feng X. Flexible triphase enzyme electrode based on hydrophobic porous PVDF membrane for high-performance bioassays. *Biosens Bioelectron*. 2021;183:113201.
- Lei Y, Sun R, Zhang X, Feng X, Jiang L. Oxygen-rich enzyme biosensor based on superhydrophobic electrode. *Adv Mater*. 2016;28(7):1477–1481.
- Song Z, Xu C, Sheng X, Feng X, Jiang L. Utilization of peroxide reduction reaction at air–liquid–solid joint interfaces for reliable sensing system construction. *Adv Mater*. 2018;30(6):1701473.
- Zhou L, Chen L, Ding Z, et al. Enhancement of interfacial catalysis in a triphase reactor using oxygen nanocarriers. *Nano Res*. 2021;14(1):172–176.
- Chen L, Sheng X, Wang D, et al. High-performance triphase biophotocatalytic assay system based on superhydrophobic substrate-supported  $\text{TiO}_2$  nanowire arrays. *Adv Funct Mater*. 2018;28(49):1801483.
- Wu Y, Feng J, Gao H, Feng X, Jiang L. Superwettability-based interfacial chemical reactions. *Adv Mater*. 2019;31(8):1800718.
- Sheng X, Liu Z, Zeng R, Chen L, Feng X, Jiang L. Enhanced photocatalytic reaction at air–liquid–solid joint interfaces. *J Am Chem Soc*. 2017;139(36):12402–12405.

18. Zhou H, Sheng X, Xiao J, et al. Increasing the efficiency of photocatalytic reactions via surface microenvironment engineering. *J Am Chem Soc.* 2020;142(6):2738-2743.
19. Jin Z, Wang L, Zuidema E, et al. Hydrophobic zeolite modification for in situ peroxide formation in methane oxidation to methanol. *Science.* 2020;367(6474):193-197.
20. Zou S, Wang D, Xiao J, Feng X. Mathematical model for a three-phase enzymatic reaction system. *Ind Eng Chem Res.* 2023;62(10):4337-4343.
21. Bird RB, Stewart WE, Lightfoot EN. *Transport Phenomena*. 2nd ed. John Wiley & Sons; 2006.
22. Sander R. Compilation of Henry's law constants (version 4.0) for water as solvent. *Atmos Chem Phys.* 2015;15(8):4399-4981.
23. Parker JW, Schwartz CS. Modeling the kinetics of immobilized glucose oxidase. *Biotechnol Bioeng.* 1987;30(6):724-735.
24. Tao Z, Raffel RA, Soud A-K, Goodisman J. Kinetic studies on enzyme-catalyzed reactions: oxidation of glucose, decomposition of hydrogen peroxide and their combination. *Biophys J.* 2009;96(7):2977-2988.
25. Bard AJ, Faulkner LR, White HS. *Electrochemical Methods: Fundamentals and Applications*. 3rd ed. John Wiley & Sons; 2022.
26. Baronas R, Ivanauskas F, Kulys J. *Mathematical Modeling of Biosensors: an Introduction for Chemists and Mathematicians*. 2nd ed. Springer; 2021.
27. Chen X-M, Xiao J, Zhu Y-P, Luo Z-H. Intraparticle mass and heat transfer modeling of methanol to olefins process on SAPO-34: a single particle model. *Ind Eng Chem Res.* 2013;52(10):3693-3707.
28. Poling BE, Prausnitz JM, O'Connell JP. *The Properties of Gases and Liquids*. 5th ed. McGraw-Hill; 2001.
29. Atkinson B, Lester DE. An enzyme rate equation for the overall rate of reaction of gel-immobilized glucose oxidase particles under buffered conditions. I. Pseudo-one substrate conditions. *Biotechnol Bioeng.* 1974;16(10):1299-1320.
30. Atkinson B, Lester DE. An enzyme rate equation for the overall rate of reaction of gel-immobilized glucose oxidase particles under buffered conditions. II. Two limiting substrates. *Biotechnol Bioeng.* 1974;16(10):1321-1343.
31. Bartlett PN, Pratt KFE. Theoretical treatment of diffusion and kinetics in amperometric immobilized enzyme electrodes part I: redox mediator entrapped within the film. *J Electroanal Chem.* 1995;397(1):61-78.
32. Zhang J, Sheng X, Ding Z, et al. Decoupling hydrogen production from water oxidation by integrating a triphase interfacial bioelectrochemical cascade reaction. *Sci Bull.* 2021;66(2):164-169.

## SUPPORTING INFORMATION

Additional supporting information can be found online in the Supporting Information section at the end of this article.

**How to cite this article:** Zou S, Xiao J, Feng X. Modeling enzymatic and electrochemical cascade reactions at the three-phase interface enzyme electrode. *AIChE J.* 2024;e18420. doi:[10.1002/aic.18420](https://doi.org/10.1002/aic.18420)